mAbs 6:5, 1314–1326; September/October 2014; © 2014 Taylor & Francis Group, LLC

The human Müllerian inhibiting substance type II receptor as immunotherapy target for ovarian cancer

Validation using the mAb 12G4

Nathalie Kersual[1,2,3,4], Véronique Garambois[1,2,3,4], Thierry Chardès[1,2,3,4], Jean-Pierre Pouget[1,2,3,4], Imed Salhi[1,2,3,4], Caroline Bascoul-Mollevi[4], Frédéric Bibeau[4], Muriel Busson[1,2,3,4], Henri Vié[5], Béatrice Clémenceau[5], Christian K Behrens[6], Pauline Estupina[1,2,3,4], André Pèlegrin[1,2,3,4], and Isabelle Navarro-Teulon[1,2,3,4,*]

[1]IRCM; Institut de Recherche en Cancérologie de Montpellier; Montpellier; France; [2]INSERM; U896; Montpellier, France; [3]Université Montpellier; Montpellier, France; [4]Institut régional du Cancer de Montpellier; ICM; Montpellier, France; [5]Institut de Recherche Thérapeutique de l'Université de Nantes; INSERM U892; Nantes, France; [6]LFB Biotechnologies; Les Ulis, France

Keywords: MISRII, immunotherapy, GCT, ovarian carcinoma, therapeutic antibodies

Abbreviations: ADCC, Antibody-Dependent Cell Cytotoxicity; EOC, epithelial ovarian cancer; GCT, granulosa cell tumors; MISRII, Müllerian inhibiting substance type II receptor; MIS, Müllerian inhibiting substance; mAb, monoclonal antibody.

Ovarian cancer has the highest mortality rate among gynecologic malignancies. The monoclonal antibody 12G4 specifically recognizes the human Müllerian inhibiting substance type II receptor (MISRII) that is strongly expressed in human granulosa cell tumors (GCT) and in the majority of human epithelial ovarian cancers (EOC). To determine whether MISRII represents an attractive target for antibody-based tumor therapy, we first confirmed by immunohistochemistry with 12G4 its expression in all tested GCT samples (4/4) and all, but one, EOC human tissue specimens (13/14). We then demonstrated in vitro the internalization of 12G4 in MISRII^{high}COV434 cells after binding to MISRII and its ability to increase the apoptosis rate (FACS, DNA fragmentation) in MISRII^{high}COV434 (GCT) and MISRII^{medium}NIH-OVCAR-3 (EOC) cells that express different levels of MISRII. A standard ^{51}Cr release assay showed that 12G4 mediates antibody-dependent cell-meditated cytotoxicity. Finally, in vivo assessment of 12G4 anti-tumor effects showed a significant reduction of tumor growth and an increase of the median survival time in mice xenografted with MISRII^{high}COV434 or MISRII^{medium}NIH-OVCAR-3 cells and treated with 12G4 in comparison to controls treated with an irrelevant antibody. Altogether, our data indicate that MISRII is a new promising target for the control of ovarian GCTs and EOCs. A humanized version of the 12G4 antibody, named 3C23K, is in development for the targeted therapy of MISRII-positive gynecologic cancers.

Introduction

Ovarian cancer is the primary cause of death by gynecologic cancer and, overall, the seventh cause of death in women worldwide.[1] It comprises an heterogeneous group of tumors that are classified as epithelial, germ cell or sex cord-stromal, based on the anatomic structure from which they presumably originate.[2] Granulosa cell tumors (GCTs) account for 70% of sex cord-stromal tumors (but represent only 3% of all ovarian cancers) and are subdivided in juvenile and adult forms based on their clinical presentation, histological characteristics and genetics (*FOXL2* gene mutation).[3,4] Although their malignant potential is relatively low in the first years of the disease, recurrences may appear up to 30 y after surgical removal of the primary tumor.[5] Epithelial ovarian cancers (EOCs) represent about 82% of all ovarian tumors. When these carcinomas are diagnosed at early stages, the 5-y survival rate is about 80%.[6] However, at diagnosis, ~75% of women have already widespread intra-abdominal disease and therefore the 5-y survival rate is poor with only about 45% of patients living beyond this time point. Standard therapies for advanced disease, such as primary cytoreductive surgery followed by chemotherapy, rarely result in long-term benefits for patients with locally advanced and metastatic disease[6] and the relapse rate is ~85%.[7] Thus, novel therapeutic approaches are needed. Considerable advances in monoclonal antibody (mAb) biotechnology and engineering have led to the development of a new class of therapeutic agents that target specific tumor-related structures to improve the selective identification and destruction of tumor cells (a list of mAbs in Phase 3 clinical studies of cancer patients can be found in ref. [8]). More than 36 clinical trials are currently

*Correspondence to: Isabelle Navarro-Teulon; Email: isabelle.teulon@inserm.fr
Submitted: 02/05/2014; Revised: 05/20/2014; Accepted: 05/21/2014
http://dx.doi.org/10.4161/mabs.29316

investigating the feasibility of antigen-specific active immunotherapy for ovarian cancer. The largest body of evidence concerns CA-125 targeted antibody therapy, but other antigens, such as CDR2, P53, GP38, mesothelin, HER-2, folate receptor-α, HMFG, MUC1, cancer-testis antigens, TAG-72, or VEGF, are also under evaluation.[9,10]

The Müllerian inhibiting substance (MIS, or anti-Müllerian hormone [AMH]) is a glycoprotein hormone of 140 kDa composed of two identical subunits. It is a member of the transforming growth factor-β (TGF-β) family that regulates tissue growth and differentiation [for a review see ref. [11]]. MIS is responsible for regression of the Müllerian ducts in male embryos, but it is also produced in both male and female gonads after birth where it plays roles in folliculogenesis,[12] adult germ cell maturation and gonadal function.[13,14] Furthermore, because of its pro-apoptotic activity MIS may also be involved in tumor control in adults. Indeed, MIS inhibits tumor cell proliferation in vitro and in vivo in breast,[15,16] prostate,[17] cervical,[18,19] endometrial,[20] and ovarian cancers[21-23] via MIS receptor-mediated mechanisms. MIS interacts with a heterodimeric receptor system consisting of single membrane-spanning serine/threonine kinase receptors of type I (MISRI) and II (MISRII).[24] MISRI is nearly ubiquitously expressed, whereas MISRII is mainly detected in the gonads and other organs of the reproductive tract. It was reported that MISRII is expressed, albeit at different levels, in 96% of human primary GCTs[25] and in human EOC cell lines, ascites cells isolated from patients and solid tumors from patients with ovarian carcinoma.[26] Specifically, these authors showed that the EOC cell lines expressing functional MISRII are responsive to the inhibitory function of MIS. They also demonstrated that MIS could bind to 56% of the derived ascites cell cultures and induce growth inhibition in 82% of them. MISRII expression was detected also in cell lines derived from other tumors, such as breast[16] or prostate cancer.[27] These results have been confirmed and extended using various human cancer cell lines and human EOC and other tumor specimens,[28-30] suggesting a very specific expression profile of MISRII in human cancers, especially in ovarian tumors. This feature could minimize the side effects of systemic anti-cancer therapies targeting the MIS-MISRI/II system.

We developed and characterized the mouse mAb 12G4 against human MISRII.[31] Here, we report the in vitro and in vivo assessment of 12G4 effects using human GCT and EOC cell lines. We show that 12G4 effectively inhibits tumor growth in nude mice xenografted with ovarian cancer cells mainly via antibody-dependent cell-mediated cytotoxicity (ADCC), although apoptosis may also be involved. Altogether, our results on the anti-tumor effects of the murine 12G4 mAb indicate that the MISRII receptor is a new promising target for the treatment of MISRII-positive GCTs and EOCs.

Results

MISRII is expressed in most types of ovarian tumors

We first evaluated the ability of the mouse mAb 12G4 to detect MISRII expression in the main subtypes of human ovarian tumors by immunohistochemistry. To correlate our results with previously published data,[28] we analyzed 20 biopsies, mainly EOC and GCT specimens at different stages of disease progression (**Table 1**). All but two tumors (a serous adenocarcinoma: sample 13; and a dysgerminoma: sample 20) expressed MISRII. In the positive EOC samples (80%), MISRII-positive cells represented on average more than 50% of tumor cells, ranging from rare to 95% of cells (**Table 1**). In the normal ovary, MISRII was expressed in follicular granulosa cells (**Fig. 1A**). In EOCs, MISRII expression was mainly detected in the cytoplasm of epithelial tumor cells, frequently with a granular pattern (**Figs. 1C and D**).

Table 1. Description and MISRII expression in cancer specimens from patients with the main subtypes of ovarian tumors (GCT: granulosa cell tumor)

Sample n°	Age	Cancer histology	FIGO stage	MISR–II Stained cells	Staining intensity
1	61	Serous adenocarcinoma	IIIc	95%	++/+++
2	59	Serous adenocarcinoma (liver metastasis)	IV	95%	++/+++
3	74	Serous adenocarcinoma	Ic	95%	+/++
4	60	Serous adenocarcinoma	IIIc	95%	+
5	70	Serous adenocarcinoma	IIIc	90%	+
6	64	Serous adenocarcinoma	IIIc	90%	++/+++
7	49	Serous adenocarcinoma	IIIc	70%	+
8	72	Serous adenocarcinoma	IIIc	60%	++
9	67	Serous adenocarcinoma	IIIc	20%	++
10	42	Serous adenocarcinoma	IIIc	rare cells	+
11	58	Serous adenocarcinoma	IIIb	rare cells	+
12	45	Serous adenocarcinoma	IIIc	rare cells	++
13	60	Serous adenocarcinoma	IIIc	0%	0
14	34	Mucinous borderline tumor	Ia	10%	+
15	54	Primary GCT	Ia	95%	++/+++
16	63	Recurrent GCT	IV	95%	+++
17	63	Recurrent GCT	IIIc	95%	+++
18	62	Recurrent GCT	IIIc	80%	+
19	39	Clear cell adecarcinoma	IIIc	95%	+++
20	31	Dysgerminoma	Ia	0%	0

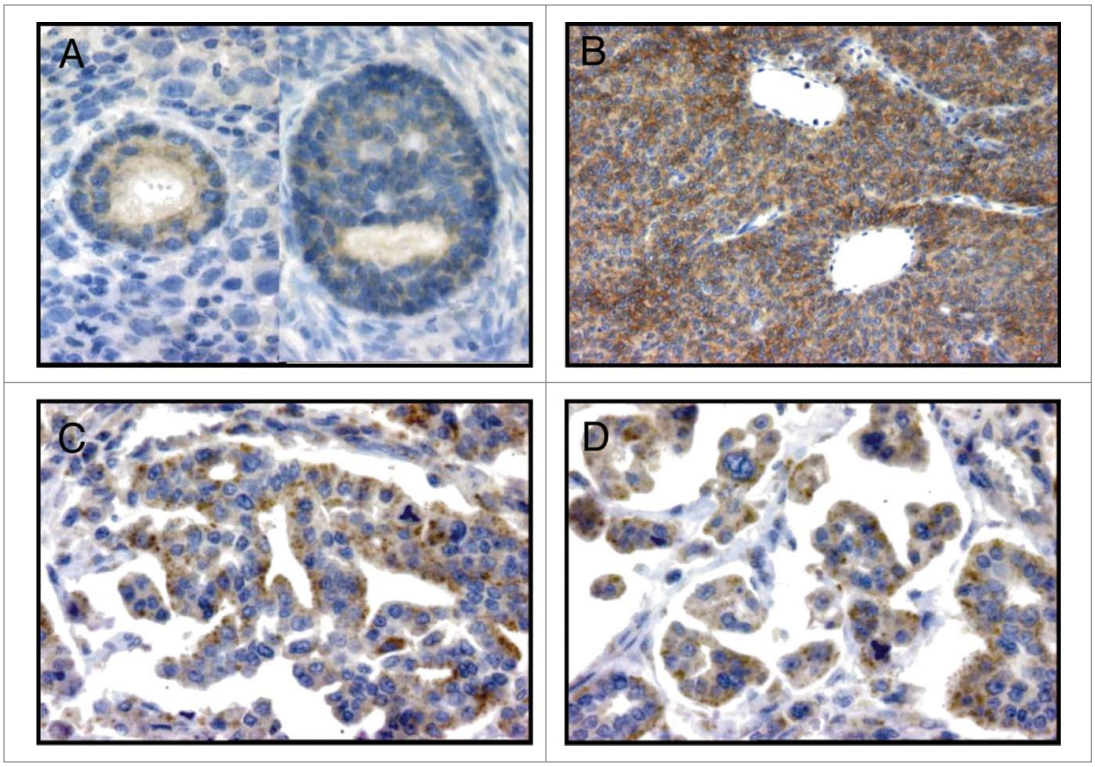

Figure 1. Immunohistochemical assessment of MISRII expression using the mAb 12G4 in (**A**) normal ovarian follicles (x 400), (**B**) granulosa cell tumor (x 400), (**C**) and (**D**) serous ovarian adenocarcinoma (x 400) specimens. In epithelial tumors (EOC), staining is moderate to strong and mainly located in the cytoplasm with a granular pattern; in granulosa cell tumors (GCT), MISRII expression is stronger and mainly at the cell membrane.

Conversely, in GCTs (**Fig. 1B**), MISRII showed a strong (more than 80% positive tumor cells), membranous expression in all examined tumors (**Fig. 1B**; **Table 1**). In the two metachronous samples from the same patient (samples 16 and 17), MISRII expression level was comparable (**Table 1**). These results strongly suggest that MISRII could be a valuable target for immunotherapy of ovarian cancer.

MISRII expression in MISRII^{high}COV434 and MISRII^{medium}NIH-OVCAR-3 cells is detected using the mAb 12G4

We then estimated MISRII level in the cell models used for this study. Flow cytometry analysis of MISRII expression in the GCT- and EOC-derived cell lines was performed using the mAb 12G4 (**Fig. 2A**). High MISRII expression was detected in MISRII^{high}COV434 (GCT) cells that were stably transfected with a MISRII construct, whereas no shift of the fluorescence peak was observed in the parental COV434 cell line (**Fig. 2A**). NIH-OVCAR-3 (EOC) cells showed a moderate MISRII expression (MISRII^{medium}NIH-OVCAR-3) (**Fig. 2A**), which corresponds to the MISRII constitutive expression profile. No binding was observed with the irrelevant 35A7 anti-carcinoembryonic antigen (CEA) mAb. Cell surface MISRII expression was then assessed using QIFIKIT®. Fluorescence quantification gave a MISRII density of 2×10^4 receptors/cell at the surface of MISRII^{high}COV434 and of 4×10^3 receptors/cell in MISRII^{medium}NIH-OVCAR-3 cells.

Western blotting (**Fig. 2B**) confirmed the strong MISRII expression in MISRII^{high}COV434 cells and the weak expression in COV434 protein lysates (band of 66 kDa). Conversely, MISRII expression in MISRII^{medium}NIH-OVCAR-3 was comparable to that of COV434 cells. This discrepancy between flow cytometry and western blot data may be due to the characteristics of each detection methods (particularly protein membrane detection by flow cytometry vs. whole cell detection by western blotting).

Then, to confirm MISRII expression also in vivo, mice were xenografted with MISRII^{high}COV434 or MISRII^{medium}NIH-OVCAR-3 cells and, when tumors reached a volume of about 600 mm^3, SPECT/CT images were acquired 48 h after intravenous injection of ^{125}I-12G4. In mice xenografted with MISRII^{high}COV434 cells, radioactivity strongly concentrated in the tumor (42% at 48 h) (**Fig. 2C**). Lower amounts of radioactivity, probably unspecific, could also be detected in heart (8%), stomach (5%), thyroid (0.5%), and bladder (1.5%). In animals xenografted with MISRII^{medium}NIH-OVCAR-3 cells, radioactivity was also detected mainly in the tumors (12% at 48 h) (**Fig. 2C**). These results confirm the constitutive level of MISRII expression in MISRII^{medium}NIH-OVCAR-3 tumor cells.

The mAb 12G4 induces receptor internalization in MISRII^{high}COV434 cells

To determine whether the 12G4-MISRII complexes formed upon binding of 12G4 to MISRII were internalized into the cells, MISRII^{high}COV434 and COV434 (negative control) cells were incubated with 10 μg/mL 12G4 at 4°C or at 37°C for 30 min, 1 h, 2 h, 3 h, or 4 h (**Fig. 3**). Internalization is exquisitely temperature-dependent and the optimal rate of ligand/receptor internalization occurs at 37°C. Indeed, while in MISRII^{high}COV434 cells incubated at 4°C, 12G4-MISRII complexes were localized exclusively at the cell membrane, in cells incubated at 37°C, they

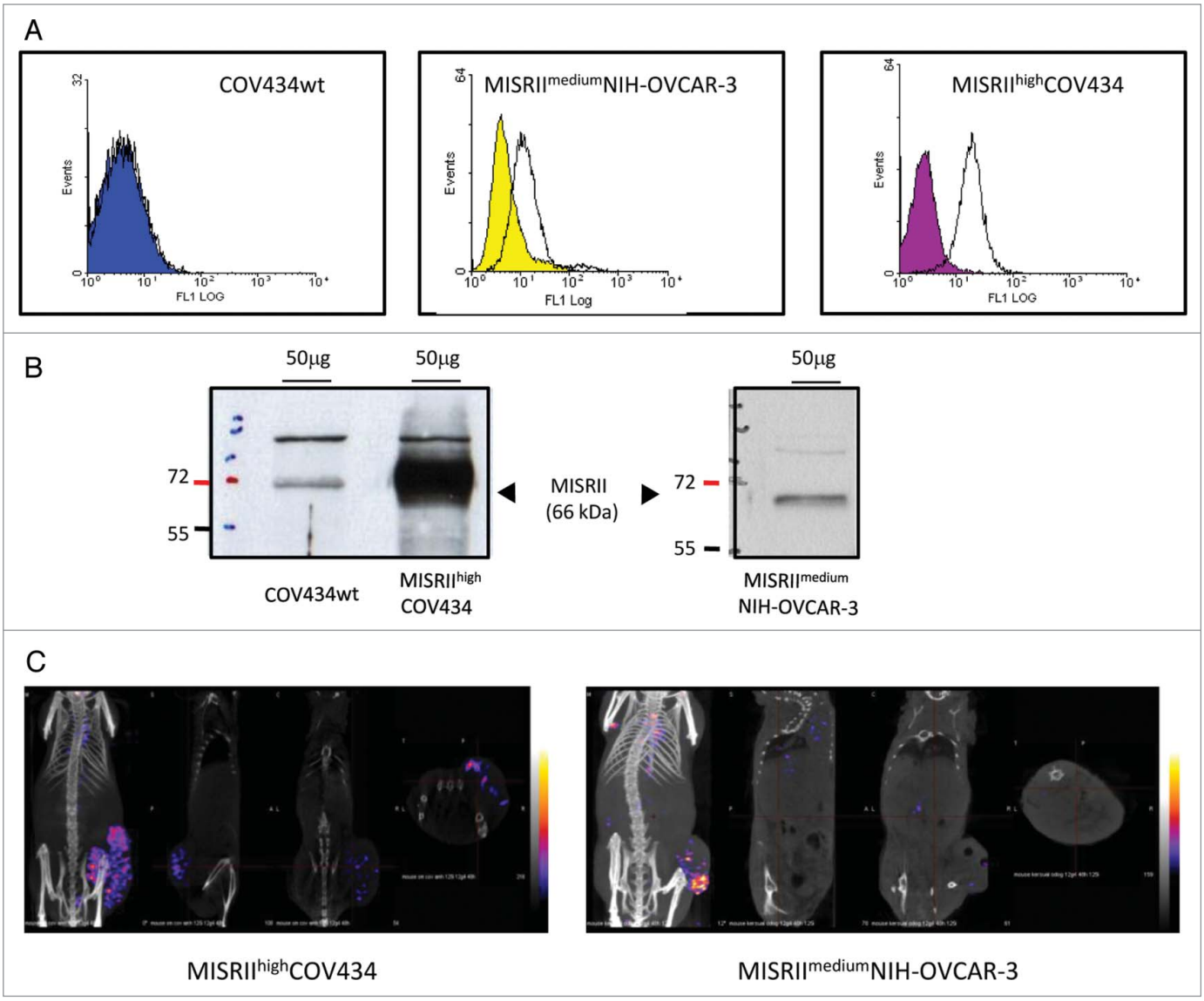

Figure 2. MISRII protein expression in GCT and EOC cell lines. (**A**) Flow cytometry analysis of 12G4 reactivity in COV434wt, MISRII^{high}COV434 and MISRII^{medium}NIH-OVCAR-3 cells. The control peak (solid color) was defined using cells incubated only with the secondary antibody. The positive population (cells incubated with the mAb 12G4) is represented by a shift of the fluorescence peak to the right. (**B**) Western blot analysis of MISRII expression in lysates from COV434, MISRII^{high}COV434 and MISRII^{medium}NIH-OVCAR-3 cells. Fifty µg of each protein extract were separated on 12% SDS-PAGE and transferred to nitrocellulose membranes. MISRII was detected using the specific mAb 12G4. The upper band in the three cell lines is non-specific, probably due to the high protein concentration of the lysates. (**C**) SPECT-CT analysis of tumors derived from MISRII^{high}COV434 or MISRII^{medium}NIH-OVCAR-3 cell xenografts. SPECT/CT images were acquired 48h after injection of ^{125}I-12G4.

were internalized, as clearly demonstrated by the presence of fluorescent cytoplasmic clusters (**Fig. 3**). Moreover, complex internalization was rapid (the cytoplasmic fluorescent staining was visible already at the 30 min time point) and persistent (still detected after 4 h). No staining was observed in COV434 control cells (COV434wt) (**Fig. 3**).

The mAb 12G4 induces apoptosis in MISRII^{high}COV434 and in MISRII^{medium}NIH-OVCAR-3 cells

To determine whether MISRII could be a target for antibody based-therapies, we asked whether, following 12G4-MISRII complex internalization, MISRII-mediated signaling pathways were activated. We thus investigated the induction of apoptosis by 12G4 in MISRII^{high}COV434 and MISRII^{medium}NIH-OVCAR-3 cells. Cells were incubated or not with 50 µg/mL 12G4 and apoptosis was quantified by FACS following staining with annexin V-FITC and PI (**Fig. 4A**). Incubation with 12G4 for 16 h strongly induced apoptosis in MISRII^{high}COV434 cells in comparison to untreated cells (7% vs. 0.5% of annexin V-positive cells and 37% vs. 2.6% of double annexinV/PI positive cells) (**Fig. 4A**). After 24h incubation, the percentage of double annexinV/PI positive cells in MISRII^{high}COV434 cells was reduced to

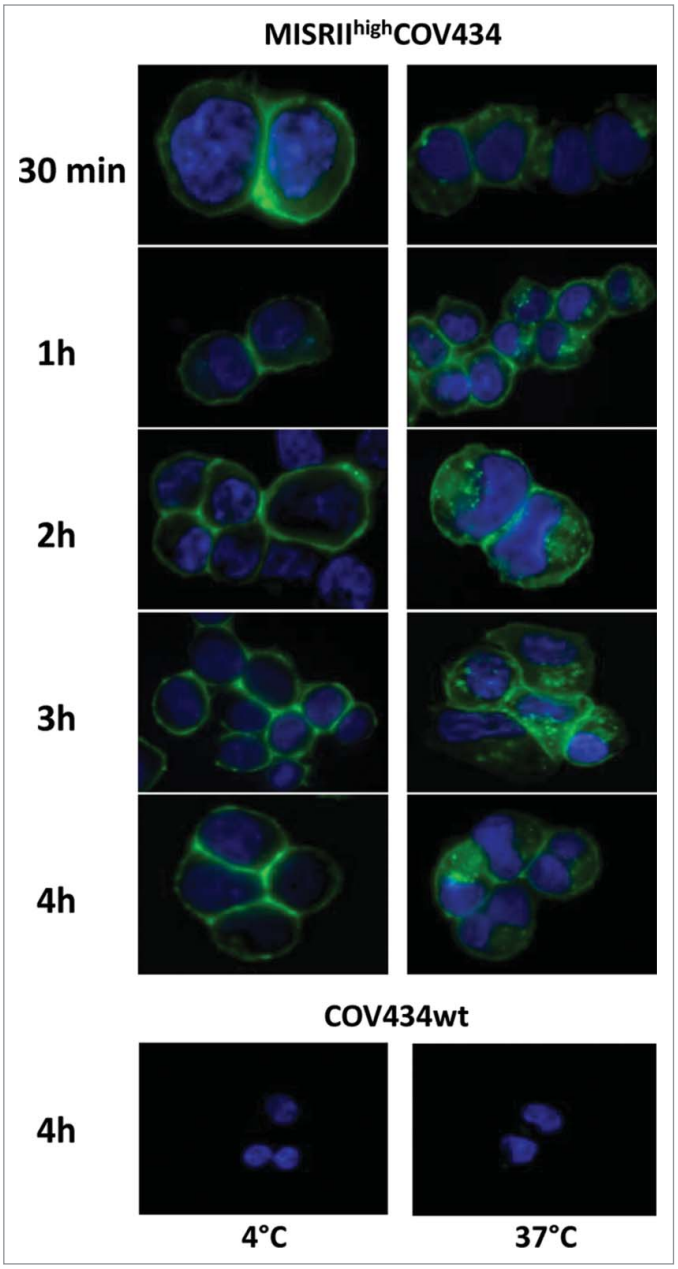

Figure 3. Analysis of 12G4 internalization by immunofluorescence MISRII^{high}COV434 or COV434 cells (COV434wt) were incubated with the mAb 12G4 at 4°C or 37°C for 30 min, 1 h, 2 h, 3 h, or 4 h. Nuclei were stained with Hoechst 33258.

22%. Conversely, in MISRII^{medium}NIH-OVCAR-3 cells, incubation with 12G4 for 16 h led to a strong increase of annexin V-positive cells (30% vs. 3.6% in untreated control) (**Fig. 4A**), but not of double annexinV/PI positive cells (4.1% vs. 1.1% in untreated cells). These results suggest that MISRII^{high}COV434 cells are in the late phases of apoptosis, whereas MISRII^{medium}-NIH-OVCAR-3 are in the early phases.[32] Therefore, we assessed the induction of apoptosis in NIH-OVCAR-3 cells also at 48h to determine whether the effect in this cell line would progress to late stage apoptosis. The results showed no apoptosis after 48h stimulation of the MISRII receptor following 12G4 binding to MISRII^{medium}NIH-OVCAR-3 cells. At this time-point (48h), MISRII^{high}COV434 cells were mainly necrotic. At all times (8, 16, and 24 h), incubation with 50 μg/mL 35A7 (irrelevant anti-CEA mAb) induced only a slight, and not significant, increase of the percentage of annexin V/PI positive cells in both MISRII^{high}-COV434 and MISRII^{medium}NIH-OVCAR-3 cells (**Fig. 4A**). Moreover, neither 12G4 nor 35A7 had any pro-apoptotic effect in COV434 cells (**Fig. 4A**).

We then used the fluorescent dye Hoechst 33258 to visualize the morphological changes associated with apoptosis. After 24h incubation of MISRII^{high}COV434 cells with 50 μg/mL 12G4, cells with the typical apoptotic features (cell shrinkage, chromatin condensation and formation of apoptotic bodies) were observed (**Fig. 4B**). The proportion of cells presenting these features was higher (about 6%) in treated than in untreated cells. Conversely, apoptotic bodies were not observed in MISRII^{medium}NIH-OVCAR-3 cells (data not shown). As nuclear fragmentation is the last event of the apoptotic process, this result is in agreement with the hypothesis that MISRII^{medium}NIH-OVCAR-3 cells are still in the early stages of apoptosis following incubation with 12G4.

These results were confirmed by flow cytometry analysis using $DiOC_6$-(3), a fluorescent lipophilic dye. Apoptosis is characterized by a reduction of the mitochondrial transmembrane potential resulting in a decrease of the emitted $DiOC_6$-(3) fluorescence. Following incubation of MISRII^{high}COV434 cells with 50 μg/mL 12G4 for 4h, the appearance of a cell population with lower $DiOC_6$-(3) fluorescence was observed (**Fig. 4C**). $DiOC_6$ fluorescence continued to decrease up to 22 h after addition of 12G4 (**Fig. 4C**). In MISRII^{medium}NIH-OVCAR-3 cells, a cell population with lower $DiOC_6$-(3) fluorescence was also detected, but only after 16 h incubation with 12G4. Altogether, these data suggest that the mAb 12G4 at high concentrations can induce moderate apoptosis in MISRII^{high}COV434 cells and, to a lesser extent, in MISRII^{medium}NIH-OVCAR-3 cells.

The mAb 12G4 shows strong ADCC

ADCC is a major mechanism by which therapeutic antibodies exert their action against cell surface targets. Therefore, we investigated whether the mAb 12G4 could induce ADCC using a ^{51}Cr release assay[33] against MISRII^{high}COV434 target (T) cells in the presence of NK92$^{mCD16h\gamma}$ effector (E) cells at different E:T ratios (**Fig. 5**). First, mouse CD16 (mCD16 hγ) expression by NK92$^{mCD16h\gamma}$ cells[34] was confirmed by flow cytometry (**Fig. 5A**). The anti-MISRII mAb 12G4, but not the mouse anti-CD20 IgG1 (negative control), could mediate ADCC against MISRII^{high}COV434 cells in a dose-dependent fashion in the presence of NK92$^{mCD16h\gamma}$ cells armed with the cognate CD16 receptor (E:T ratio = 30:1) (**Fig. 5B**). Finally, experiments performed using 5 μg/ml 12G4 and four different E:T ratios (30:1, 10:1, 3:1 and 1:1) showed that the ADCC activity was still high at a 10:1 ratio (**Fig. 5C**).

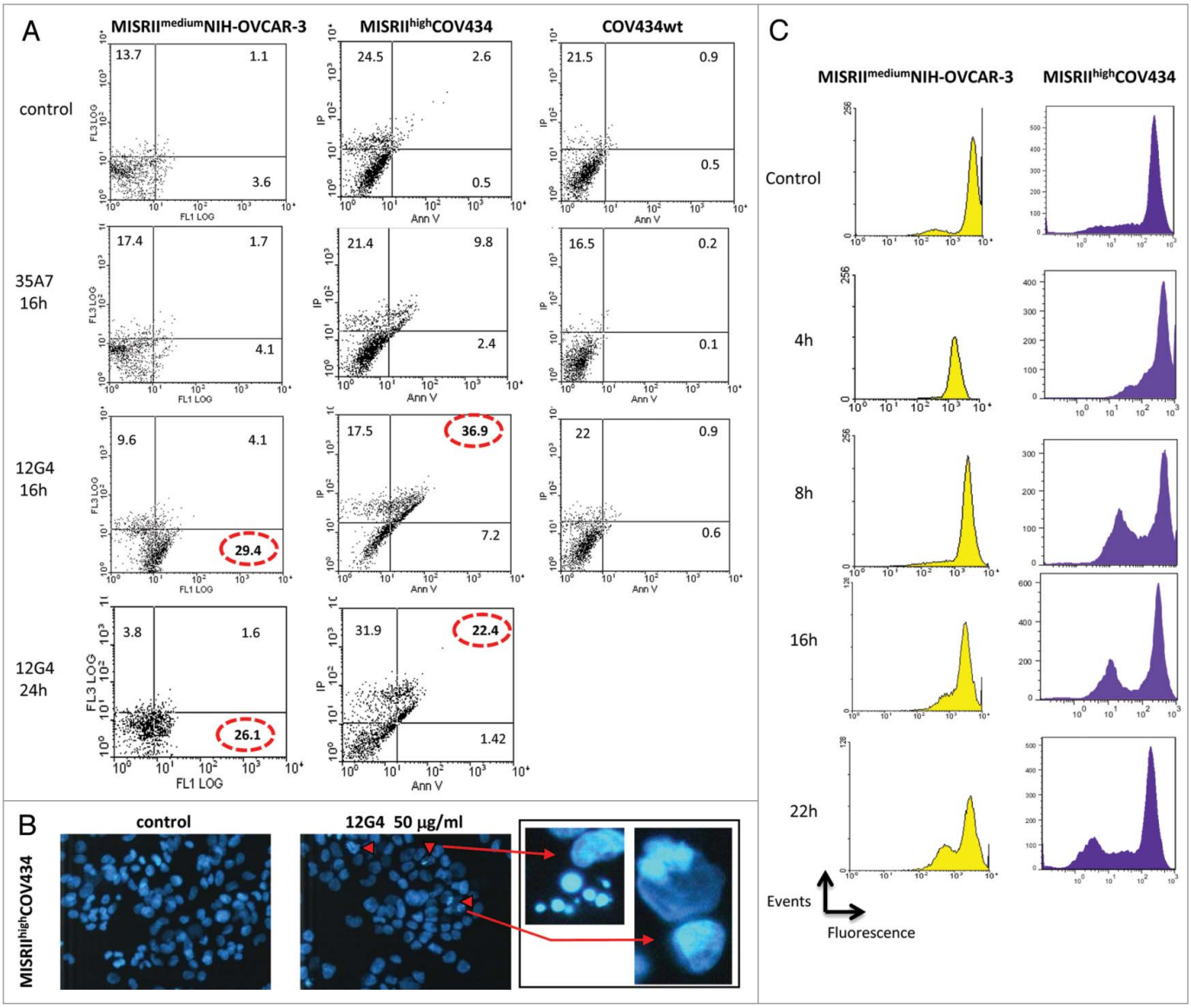

Figure 4. The mAb 12G4 induces apoptosis of MISRII^{medium}NIH-OVCAR-3 and MISRII^{high}COV434 cells, but not of COV434 cells. (**A**) Cells were incubated or not with 50 µg/mL 12G4 for 16 h and 24 h or with 50 µg/mL 35A7 (irrelevant antibody) for 16 h and then the apoptosis rate was quantified by flow cytometry following Annexin V/propidium iodide (PI) staining. (**B**) Representative fluorescence images of MISRII^{high}COV434 cells incubated or not with 50 µg/ml of 12G4 for 24 h. Apoptotic cells (arrows) have bright blue condensed or fragmented nuclei stained by Hoechst 33258. (**C**) DIOC6 (fluorescent lipophilic dye) assay at 4 h, 8 h, 16 h, and 22 h after incubation with 50 µg/mL 12G4. The decrease of the fluorescence peak corresponds to the inhibition of the mitochondrial membrane potential following apoptosis.

The mAb 12G4 inhibits tumor growth in nude mice xenografted with MISRII^{high}COV434 or MISRII^{medium}NIH-OVCAR-3 cells

Finally, to test the efficacy of immunotherapy with the mAb 12G4 in vivo, female athymic nude mice were injected subcutaneously (s.c.) with COV434, MISRII^{medium}NIH-OVCAR-3, or MISRII^{high}COV434 cells. The different level of MISRII expression in these cell lines also allowed assessment of whether MISRII expression level, which can vary in ovarian tumors, may influence the cancer cell sensitivity to 12G4. A 125 µg dose (5 mg/kg) of 12G4 (treated group) or of the anti-digoxin 2C2 mAb (control group) was injected intraperitoneally (i.p.) three times a week for 6 wk starting when tumors reached a minimum size of 80 mm^3 (at day 12, 18, and 20 post-graft for animals xenografted with MISRII^{high}COV434, COV434 and MISRII^{medium}NIH-OVCAR-3 cells, respectively). The median survival time was defined as the time when 50% of mice had a tumor of 2,000 mm^3 in size and were euthanized. 12G4 significantly slowed down the growth of tumors in animals xenografted with MISRII^{high}COV434 cells ($P < 0.001$) and increased the median survival time (46 d vs. 34 d; $P = 0.011$) compared with the irrelevant mAb (**Fig. 6A**). The growth of tumors in animals xenografted

with MISRII^{medium}-NIH-OVCAR-3 (EOC) cells was significantly slower in the group treated with 12G4 than in mice injected with the irrelevant antibody ($P = 0.012$). The median survival time was also significantly ($P = 0.001$) longer (92 d) in 12G4-treated mice than in control mice (68 d) (**Fig. 6B**). These results demonstrate that, despite the low level of MISRII expression in MISRII-^{medium}NIH-OVCAR-3 cells, 12G4 had an anti-tumor effect (68 d vs. 92 d; $P = 0.001$). In animals xenografted with COV434 cells, no significant effect of 12G4 was observed on tumor progression ($P = 0.617$) and survival ($P = 0.687$), compared with the control group (**Fig. 6C**), probably due to the very low level of MISRII expression in these tumors. However, the median survival time in the control groups was longer in mice xenografted with COV434 (68 d) than in those xenografted with MISRII^{high}COV434 cells (34 d). This may be explained by the fact that the in vitro doubling time of MISRII^{high}COV434 cells is 1.5-fold higher than that of COV434 cells, because MISRII expression confers a more aggressive status to the tumor cells or because the transfection and selection process resulted in a faster growing clone (without direct relation to the MISRII expression level). Accordingly, at day 30 post-graft, the mean size of COV434 cell-derived tumors treated with the irrelevant mAb was about 250 mm^3, whereas MISRII^{high}COV434 tumors had already reached the critical volume of 2000 mm^3 (**Fig. 6**).

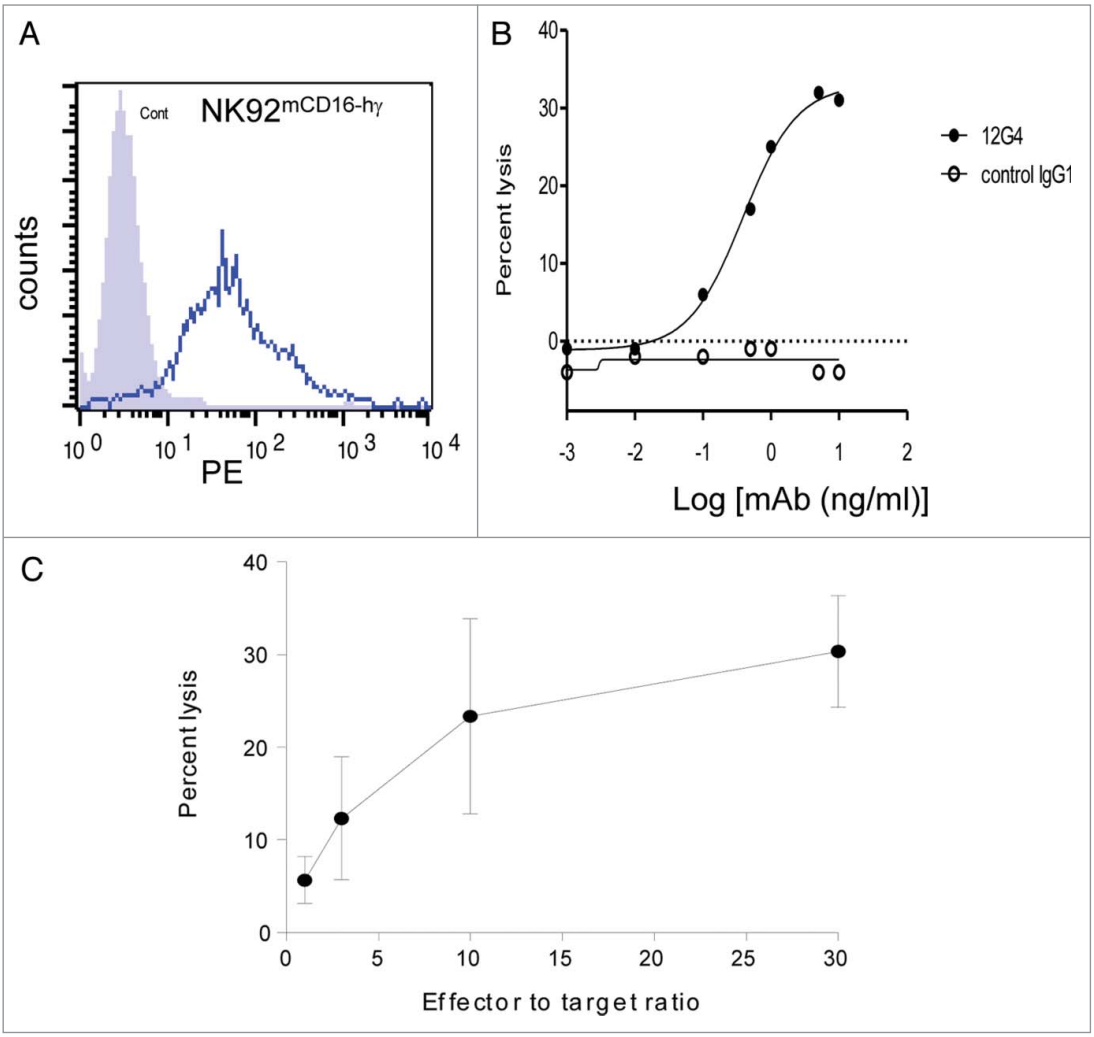

Figure 5. The mouse mAb 12G4 causes ADCC. ADCC was assessed using a standard ^{51}Cr release assay against the target cell line (MISRII^{high}COV434 cells) in the presence of NK92^{mCD16} effector cells. (**A**) Detection by flow cytometry of mouse CD16 (mCD16) in NK92^{mCD16} cells. (**B**) The mouse anti-MISRII mAb 12G4 can mediate ADCC against MISRII^{high}COV434 cells in a dose-dependent fashion in the presence of NK92 cells armed with the cognate CD16 receptor (effector:target ratio = 30:1). A mouse IgG1 against CD20 was used as negative control. (**C**) ADCC quantification following incubation with 5 μg/ml 12G4 (assay performed at four effector:target ratios). Results are expressed as the percentage of specific MISRII^{high}-COV434 cell lysis (mean ± SD of three independent experiments).

Altogether, these data clearly indicate that i.p. administration of the mAb 12G4 is effective in inhibiting tumor growth and in prolonging the median survival of mice xenografted with MISRII-positive GCT or EOC cells. They also show that the in vivo response goes in line with the target antigen expression level.

Discussion

Despite aggressive debulking surgery, chemotherapy drugs and intraperitoneal therapies, new strategies for the management of ovarian cancer are crucially needed due to its very poor prognosis. Targeted therapies of ovarian cancers with different mAbs have been tested in pre-clinical and clinical trials.[35] Promising immunological responses have been reported for most of the antibodies under study, but often they do not coincide with clinical benefits for patients with ovarian cancer.[35] Although bevacizumab (Avastin®) is approved in the EU for advanced EOC, advanced cancer of the fallopian tube or of the peritoneum (the membrane lining the abdomen) in combination with carboplatin and paclitaxel, and in Japan as well as other countries for ovarian cancer, new targets for

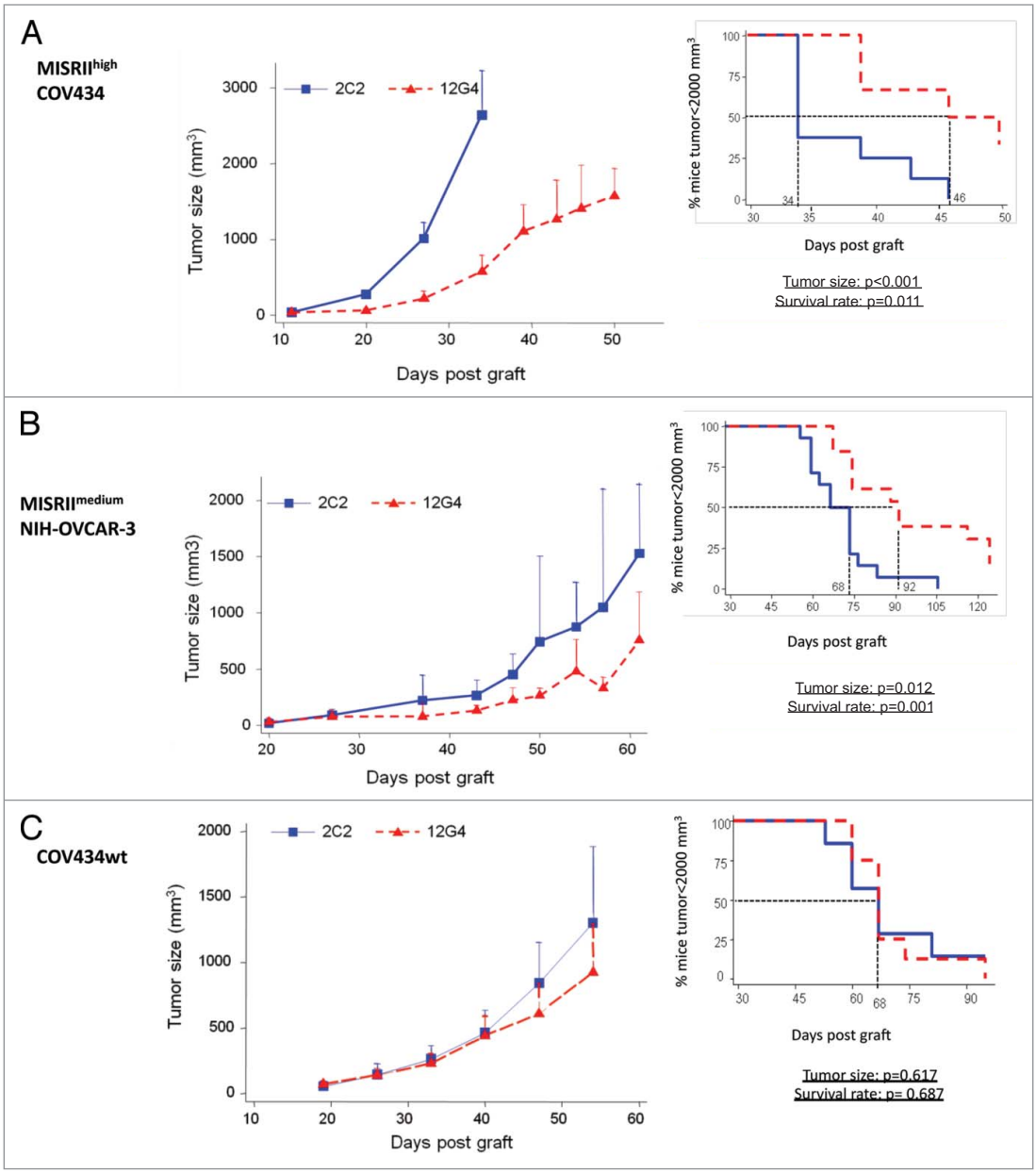

Figure 6. In vivo efficacy of the mAb 12G4 in nude mice xenografted with (**A**) MISRII^{high}-COV434, (**B**) MISRII^{medium}NIH-OVCAR-3 or (**C**) COV434 cells. Results are presented as tumor growth curves (mean +95% CI upper bound) and as a Kaplan–Meier survival curves (percentage of mice with a tumor volume lower than 2,000 mm^3 as a function of time after graft). The solid line corresponds to treatment with the irrelevant 2C2 mAb, dotted line corresponds to treatment with 12G4.

antibody therapy are urgently needed. MISRII, which is expressed in most subtypes of human ovarian carcinomas, might be one of them. In the present study, we assessed the in vivo and in vitro effects of the mAb 12G4 that specifically recognizes human MISRII.

We previously demonstrated by immunohistochemistry MISRII expression in human GCTs and in human testis (cytoplasmic staining in Sertoli and Leydig cells).[31] In the present study, using the mAb 12G4, we show that MISRII is expressed in follicular granulosa cells of normal ovary, as well as in 80% of tested EOC and all GCT specimens from patients at different stages of disease. Although concerning a small series (n = 20), these results demonstrating that MISRII is expressed in different types of ovarian tumors (EOC, borderline and GCT) are in agreement with previous studies.[25,28] Indeed, MISRII was expressed in serous and clear cell adenocarcinoma (i.e., malignant EOCs) and also in adult GCTs (i.e., sex cord-stromal tumors). If MISRII is going to be targeted by immunotherapy approaches, antibody treatments could induce side effects in normal tissues that express MISRII. However, Bakkum-Gamez et al.[28] reported low levels of MISRII expression in select non-gynecologic tissues. Moreover, MISRII expression in the normal ovary of patients with ovarian carcinoma should also not be a problem theoretically because, following the diagnosis ovarian ablation by hormone manipulation, surgery or radiotherapy is often performed.

We then show that 12G4-MISRII complexes are internalized into the cytoplasm of GCT cells. Internalization of cell surface receptors is mediated either by clathrin- or non-clathrin-mediated endocytic pathways. MIS receptors belong to the TGF-β receptor family, which has been extensively studied in terms of internalization/recycling/degradation routes.[36,37] Internalization of such receptors by clathrin-dependent endocytosis increases TGFβ signal transduction, whereas internalization via clathrin-independent lipid raft-mediated endocytosis promotes their degradation through SMAD7/SMURF2-mediated ubiquitination.[38] By analogy, we postulated that the mAb 12G4 could act by modulating signaling/degradation pathways following receptor internalization. Indeed, 12G4 stimulated apoptosis in both

MISRII^{high}COV434 and MISRII^{medium}NIH-OVCAR-3 cell lines. MIS-induced cell apoptosis was previously described in EOC cell lines, such as OVCAR-5 and OVCAR-8 cells.[26,39] Moreover, Anttonen et al.[25] showed that incubation with MIS promoted activation of caspase-3 in a concentration-dependent manner and apoptosis in a human GCT cell line and in primary cell cultures of human GCTs.

Beside activation of signaling/degradation pathways following receptor internalization, here we describe the strong ADCC effect of 12G4 on MISRII-positive COV434 cells, thereby demonstrating that 12G4 is able to mediate cytotoxicity via effector cell-dependent mechanisms. Clynes et al.[40] have shown that the Fc-mediated effects of trastuzumab were related to ADCC because both nude and SCID mice have functioning macrophages and NK cells capable of killing tumor cells by ADCC.[41] In the present study, the 12G4 antibody inhibited tumor growth in mice xenografted with MISRII^{high}COV434 cells, and to a lesser extent also in animals xenografted with MISRII^{Medium}NIH-OVCAR-3 cells, in agreement with the lower MISRII expression level in these cells. No effect was observed on tumors derived from COV434 cells. These data indicate that although the level of MISRII expression at the cell surface influences the efficiency of the antibody, a moderate expression of about 4×10^3 receptors/cell (as determined by flow cytometry analysis) is sufficient to allow a significant anti-tumor effect. Due to the specificity of the antibody for the human receptor, it was not possible to evaluate the treatment safety in xenografted mice. However, the strong tissue-specificity of the receptor argues in favor of the potential safety of treatment with the mAb 12G4.

Taken together, our results show that the MISRII-specific mAb 12G4 may act directly in cancer cell signaling and indirectly via the immune system. Indeed, beside its anti-tumoral effect via the Fc portion, 12G4 also seems to induce cell surface MISRII receptor internalization that triggers a cascade of signaling events leading to a moderate increase of cell apoptosis. This might also contribute to the in vivo effect of the antibody, but may vary depending on the genetic background of the tumors.

In conclusion, the results of this study suggest that MISRII represents a suitable target for the treatment of ovarian cancers of various histological subtypes. The anti-tumor effects observed upon 12G4 binding to its receptor indicate that it could represent a promising tool for therapy. This antibody could also be used to detect and monitor MISRII expression or to study its turn-over at the cell membrane. The development of a humanized version of the anti-MISRII antibody 12G4, named 3C23K, is ongoing and could represent a promising new targeted approach for the therapy of ovarian and other gynecologic MISRII-positive cancers.

Materials and Methods

Cell lines and cell culture

The human GCT cell line COV434[42,43] was a kind gift from Peter I. Schrier (Department of Clinical Oncology, Leiden University Medical Center). The COV434 cell line (low MISRII expression) and a clone that stably express high MISRII levels (MISRII^{high}COV434) were grown in DMEM F12 medium. The NIH-OVCAR-3 human EOC cell line (with a constitutive moderate expression of MISRII, MISRII^{medium}NIH-OVCAR-3) was from ATCC and was maintained in RPMI 1640 medium. All media contained 10% heat-inactivated fetal bovine serum, 0.1 mg/ml streptomycin, 0.1 IU/ml penicillin and 0.25 μg/ml amphotericin B. MISRII^{high}COV434 cells were supplemented with 0.33 mg/ml geneticin. Cells were grown at 37°C in a humidified atmosphere with 5% CO_2 and medium was replaced twice a week. Cells were harvested with 0.5 mg/ml trypsin/0.2 mg/ml EDTA. All culture media and supplements were purchased from Life Technologies, Inc. (Gibco BRL).

Generation of the MISRII^{high}COV434 cell line

The cDNA coding for full-length human MISRII in the pCMV6 plasmid was a generous gift by José Teixeira (Pediatric Surgical Research Laboratories, Massachusetts General Hospital, Harvard Medical School). MISRII was first subcloned in the pcDNA3.1.myc-His vector (Invitrogen) using the EcoRI and *Xho*I restriction sites (enzymes from New England BioLabs) and then, using the EcoRI and SalI sites, in the pIRES1-EGFP vector, a kind gift from Francis Poulat (IGH-UPR1142 CNRS). Twenty-four hours before transfection, COV434 cells were seeded in a 10 cm petri dish at 80% of confluence. The MISRII construct was transfected using the Fugene transfection kit according to the manufacturer's protocol. After 48 h, the medium was replaced with fresh medium containing 500 μg/ml geneticin and was then changed twice/week for two weeks. Cells were then harvested and sorted using a FACSAria cytometer (Becton Dickinson) in 96-well plates. The COV434–1F3 clone was selected based on its strong MISRII expression (designed as MISRII^{high}COV434 cells in the manuscript).

Antibodies

The specific anti-MISRII mAb 12G4 was previously described.[31] For in vivo experiments, the anti-digoxin mAb 2C2[44] was used as irrelevant antibody. For in vitro experiments, the mAb 35A7 against the CEA Gold 2 epitope[45] was used as a control. These three mouse IgG_1 mAbs were purified from mouse hybridoma ascites by ammonium sulfate precipitation (45% saturation at 4°C), followed by ion-exchange chromatography on DE52 cellulose (Whatman) for 35A7, or by protein G affinity chromatography (12G4 and 2C2).

Immunocytochemistry

Representative tissue sections of the main subtypes of ovarian tumors were analyzed as previously described.[31] MISRII expression was assessed by using the mAb 12G4 and the DakoCytomation Envision detection system according to the manufacturer's recommendations. The negative control consisted of a slide incubated with an irrelevant mouse IgG1 antibody. A semi-quantitative evaluation was performed by two independent operators, reporting both staining intensity (weak, moderate and strong) and the percentage of stained tumor cells.

Flow cytometry analysis
MISRII expression

MISRII expression in the COV434 and NIH-OVCAR-3 cell lines was analyzed by flow cytometry. About 5×10^5 cells were incubated at 4°C with 10 μg/ml 12G4, 35A7 (irrelevant mAb) or PBS/0.1% BSA alone (control for cell auto-fluorescence) for 1.5 h. After washing, cells were incubated with fluorescein-conjugated goat anti- mouse total IgGs (1:100; Millipore) at 4°C for 1 h; after two washes, cells were analyzed (20 000 cells/analysis) using a Coulter® Epics XL-MCL™ flow cytometer (Beckman Coulter).

MISRII quantification

Quantification of MISRII cell surface expression in COV434, MISRII^{high}COV434 and MISRII^{medium}NIH-OVCAR-3 cells was performed using QIFIKIT® (DakoCytomation) that contains calibration beads coated with well-defined quantities of mouse mAbs. Briefly, cells were incubated with 12G4 at a saturating concentration (20 μg/ml). Under these conditions, the number of bound primary antibody molecules corresponds to the number of antigenic sites present at the cell surface. After washing, cells and calibration beads were independently incubated with the secondary antibody to correlate the fluorescence intensity with the number of bound primary antibody molecules on the cells and on the beads. Samples were analyzed with a Coulter® Epics XL-MCL™ flow cytometer (Beckman Coulter) and results expressed as the antibody binding capacity (ABC) of each sample.

Western blot analysis

Cells were washed and incubated at 4°C in lysis buffer (10 mM EDTA, 5 mM $MgCl_2$, 100 mM sodium vanadate, 1% Triton X100, 40 mM NaPPI, 50 mM NaF, 40 mM Tris pH8) with a cocktail of protease inhibitors (Sigma) for 20 min. The insoluble fraction was eliminated by centrifugation and the protein concentration determined using the BCA assay protein quantitation kit (Interchim). Then, cell extracts were heated at 100°C for 5 min, separated (50 μg/well) by 12% SDS-PAGE under reducing conditions (5% 2β-mercaptoethanol) and transferred to PVDF membranes (Millipore Co., Bedford, MA). Membranes were saturated in Tris/NaCl buffered saline, containing 0.1% Tween 20 and 5% non-fat dry milk, and probed with 10 μg/ml 12G4. After washing, a peroxidase-conjugated anti-mouse IgG secondary antibody (1:5000; Sigma) was added and, after washing, the antibody-antigen interaction was detected using a chemiluminescent substrate (Perkin Elmer). To verify equal loading, immunoblots were also probed with a monoclonal anti-GAPDH antibody (Millipore).

SPECT-CT analysis

When tumors reached a volume of about 600 mm^3, xenografted mice were intravenously injected with 500 μCi ^{125}I-12G4 and after 48 h whole-body SPECT/CT images were acquired using a two-headed multiplexing multi-pinhole NanoSPECT imager (Bioscan Inc., Washington DC). The pinholes aperture was 1 mm. The energy window was centered at 28 keV with ± 20% width, acquisition times were defined to obtain 30 000 counts for each projection with 24 projections. Concurrent micro-CT whole-body images were acquired for anatomic co-registration with the SPECT data. Reconstructed data from SPECT and CT imaging were visualized and co-registered using Invivoscope®. Images and maximum intensity projections (MIPs) were reconstructed using the dedicated Invivoscope® (Bioscan, Inc.) and Mediso InterViewXP® software programs (Mediso).

Internalization study
Immunofluorescence assay

Internalization of the mAb 12G4 in MISRII^{high}COV434 and COV434 cells was assessed by immunofluorescence. For each assay, 5×10^3 cells were grown on 22-mm square glass coverslips in 35-mm petri dishes with RPMI. Two days later (exponential phase of growth), cells were incubated with 10 μg/mL 12G4 in PBS/0.1% BSA at 4°C or at 37°C for 30 min, 1 h, 2 h, 3 h, or 4 h. Supernatants were removed and cells washed twice with PBS/0.1% BSA and once with PBS. Cells were then fixed in 3.7% *p*-formaldehyde/PBS for 20 min and permeabilized in acetone at –20°C for 30 s. Cells were washed twice with PBS/0.1% BSA and incubated in the dark with an FITC-labeled goat anti-mouse Ig $F(ab')_2$ fragment (Silenus, Eurobio, France) in PBS/0.1% BSA for 1 h. Then, they were washed three times with PBS/0.1% BSA and once with PBS and incubated with 50 μl 4,6 diaminido-2-phenylindole dihydrochloride (DAPI, Sigma, Chemical Co.) for 15 min, washed once with PBS and prepared for fluorescent microscopic visualization by using Vectashield®.

Hoechst staining

Five $\times 10^4$ cells were plated on glass coverslips in 24-well culture plates. At the end of the treatment period, cells were washed twice with PBS and fixed with 4% paraformaldehyde for 15 min. After washing in PBS, slides were then incubated with 50 ng/ml Hoechst 33258 (Sigma) in the dark for 5 min. Cells were washed three times, mounted with a fluorescent mounting medium (Dako) and examined using a Zeiss Axioplan microscope.

Detection of apoptosis
Annexin V assay

Approximately 350 000 cells were seeded in 6-well culture plates and incubated or not with 50 μg/ml 12G4 for 16h or 24h and then stained using the annexin V-FITC Apoptosis Detection Kit (Roche). Briefly, both adherent and detached cells were collected and centrifuged at 1,000 rpm for 5 min. After washing with PBS, cells were stained with 100 μL of a mix containing FITC-labeled annexin V and propidium iodide (PI) in annexin buffer (10 mM Hepes/NaOH, 140 mM NaCl, 5 mM $CaCl_2$, pH 7.4) and incubated in the dark at room temperature for 10 min. After addition of 600 μL binding buffer, cells were analyzed by flow cytometry and data analyses performed using the CELLQuest software (Beckton-Dickinson).

DiOC6 (3,3′- dihexyloacarbocyanine iodide) assay

Approximately 500 000 cells were seeded in 6-well culture plates, incubated or not, with 50 μg/ml 12G4 for 4, 8, 16, and 24 h and then were washed with PBS. 1×10^5 cells were resuspended in 500 μl PBS and incubated with 1 μl of 40 nM $DiOC_6(3)$ (dissolved in DMSO), a cationic fluorescent dye which strongly labels mitochondria, in the dark at room temperature for 30 min before flow cytometric analysis. A decrease of the mitochondrial transmembrane potential (MTP) in apoptotic cells is associated with a reduction of $DiOC_6(3)$ uptake. $DiOC_6(3)$ was purchased from Sigma-Aldrich.

ADCC measurement

Cytotoxic activity was assessed using a standard ^{51}Cr release assay.[33] $MISRII^{high}COV434$ target cells were labeled with 100 μCi ^{51}Cr at 37°C for 1 h, washed four times with culture medium and then plated at 30:1, 10:1, 3:1 or 1:1 effector-to-target cell ratio in a 96-well flat-bottom plate. Cells were then incubated with the anti-MISRII mouse mAb 12G4 or an irrelevant anti-CD20 IgG1 mAb for 20 min before addition of $NK92^{mCD16}$ effector cells (NK92 cells transduced with mouse CD16 hγ that was stably expressed at the cell surface).[34] After 4-h incubation at 37°C, a 25 μl aliquot of supernatant was removed from each well, mixed with 100 μl scintillation fluid and ^{51}Cr activity counted in a scintillation counter (MicroBeta; Perkin Elmer). Each test was performed in triplicate. The results are expressed as the percentage of lysis, which is calculated according to the following equation: (experimental release-spontaneous release) / (maximal release-spontaneous release) × 100, where the experimental release represents the mean counts per minute (cpm) for the target cells in the presence of the effector cells, the spontaneous release represents the mean cpm for target cells incubated without effector cells, and the maximal release represents the mean cpm for target cells incubated with 1% Triton X100 (Sigma).

In vivo study

All animal experiments were performed in compliance with the guidelines of the French government and the regulations of the Institut National de la Santé et de la Recherche Médicale for experimental animal studies (agreement B34–172–27). Cells used for xenografts were resuspended in culture medium alone ($MISRII^{medium}$NIH-OVCAR-3 cells) or in 50% medium and 50% Matrigel (BD Biosciences) (COV434 and $MISRII^{high}$-COV434 cells). Ten million cells/mice were inoculated s.c. into the right flank of 6−8 wk old female athymic nude mice purchased from Harlan. When tumors reached a minimum size of 80 mm^3, mice were randomized to the different treatment groups: $MISRII^{high}COV434$-, $MISRII^{medium}$NIH-OVCAR-3- and COV434wt-xenografted mice treated with 12G4 (6, 13, and 8 animals/group, respectively) and mice treated with the 2C2 irrelevant antibody (8, 14, and 7 animals/group, respectively). Mice were i.p. injected with 125 μg of the anti-MISRII mAb 12G4 or of the irrelevant 2C2 mAb three times a week for six consecutive weeks. Thus, a total dose of 2250 μg mAb/mouse was injected over the six-week period. Tumor dimensions were measured once a week with a caliper and volumes calculated using the formula: $D_1 \times D_2 \times D_3$ /2. Tumor progression was assessed using the formula [(final volume) - initial volume] / (initial volume). Results were also expressed with an adapted Kaplan-Meier survival curve, using the time needed for a tumor to reach the volume of 2000 mm^3. The median survival was defined as the time when 50% of mice had a tumor of that volume.

Human ovarian cancer specimens

Ovarian cancer specimens were from patients treated at the Institute of Cancer of Montpellier (ICM), France. All patients gave their informed consent for the use of human material for research purposes and this research project was approved by the local ethics committee. The ovarian tumors were classified and described according to the recent World Health Organization tumor classification systems.[46] They were mainly EOCs and GCTs (**Table 1**): serous adenocarcinoma (n = 13), clear cell adenocarcinoma (n = 1), mucinous borderline endocervical-like tumor (n = 1), dysgerminoma (n = 1) and primary (n = 1) or recurrent (n = 3) adult GCTs. Among the patients with malignant EOC (i.e., serous adenocarcinoma and clear cell adenocarcinoma), one had stage I, 12 stage III, and one stage IV (liver metastasis) disease according to the FIGO classification. GCT specimens were from stage I (n = 1), stage III (n = 2), and stage IV (n = 1) tumors. Two recurrent GCTs were collected from the same patient at different times of tumor progression. One normal ovary was also examined.

Statistical analysis

A linear mixed regression model was used to determine the relationship between tumor growth and days post-graft. The fixed part of the model included variables corresponding to the number of days post-graft and the different groups. Interaction terms were built into the model. Random intercept and random slope were included to take into account the time effect. The coefficients of the model were estimated by maximum likelihood and considered significant at the 0.05 level. Survival rates were estimated from the xenograft date until the date when the tumor reached a volume of 2000 mm^3 using the Kaplan–Meier method. Median survival was presented with 95% confidence intervals. Survival curves were compared using the log-rank test. Statistical analysis was performed using the STATA 11.0 software.

Disclosure of Potential Conflicts of Interest

No potential conflicts of interest were disclosed.

Acknowledgments

We acknowledge the expert technical assistance of Sabine Bousquié, Geneviève Heintz, and Imade Aït-Arsa. We also thank Jean-Marc Barret for critical reading of the manuscript.

Funding

This work was supported by grants from LFB Biotechnologies. N.K. was also supported by a fellowship from LFB Biotechnologies. This work was supported by the program "Investissement d'avenir" grant agreement: Labex Mabimprove, ANR-10-LABX-5301.

References

1. Jemal A, Siegel R, Ward E, Hao Y, Xu J, Thun MJ. Cancer statistics, 2009. CA Cancer J Clin 2009; 59:225-49; PMID:19474385; http://dx.doi.org/10.3322/caac.20006
2. La Marca A, Volpe A. The Anti-Mullerian hormone and ovarian cancer. Hum Reprod Update 2007; 13:265-73; PMID:17213257; http://dx.doi.org/10.1093/humupd/dml060
3. Jamieson S, Butzow R, Andersson N, Alexiadis M, Unkila-Kallio L, Heikinheimo M, Fuller PJ, Anttonen M. The FOXL2 C134W mutation is characteristic of adult granulosa cell tumors of the ovary. Mod Pathol 2010; 23:1477-85; PMID:20693978; http://dx.doi.org/10.1038/modpathol.2010.145
4. Shah SP, Köbel M, Senz J, Morin RD, Clarke BA, Wiegand KC, Leung G, Zayed A, Mehl E, Kalloger SE, et al. Mutation of FOXL2 in granulosa-cell tumors of the ovary. N Engl J Med 2009; 360:2719-29; PMID:19516027; http://dx.doi.org/10.1056/NEJMoa0902542
5. Singh-Ranger G, Sharp A, Crinnion JN. Recurrence of granulosa cell tumour after thirty years with small bowel obstruction. Int Semin Surg Oncol 2004; 1:4; PMID:15285808; http://dx.doi.org/10.1186/1477-7800-1-4
6. Ozols RF, Bundy BN, Greer BE, Fowler JM, Clarke-Pearson D, Burger RA, Mannel RS, DeGeest K, Hartenbach EM, Baergen R; Gynecologic Oncology Group. Phase III trial of carboplatin and paclitaxel compared with cisplatin and paclitaxel in patients with optimally resected stage III ovarian cancer: a Gynecologic Oncology Group study. J Clin Oncol 2003; 21:3194-200; PMID:12860964; http://dx.doi.org/10.1200/JCO.2003.02.153
7. Gordon AN, Schultes BC, Gallion H, Edwards R, Whiteside TL, Cermak JM, Nicodemus CF. CA125- and tumor-specific T-cell responses correlate with prolonged survival in oregovomab-treated recurrent ovarian cancer patients. Gynecol Oncol 2004; 94:340-51; PMID:15297171; http://dx.doi.org/10.1016/j.ygyno.2004.04.024
8. Reichert JM. Antibodies to watch in 2014. MAbs 2014; 6:5-14; PMID:24284914
9. Kandalaft LE, Powell DJ Jr., Singh N, Coukos G. Immunotherapy for ovarian cancer: what's next? J Clin Oncol 2011; 29:925-33; PMID:21079136; http://dx.doi.org/10.1200/JCO.2009.27.2369
10. Oei AL, Sweep FC, Thomas CM, Boerman OC, Massuger LF. The use of monoclonal antibodies for the treatment of epithelial ovarian cancer (review). [review]. Int J Oncol 2008; 32:1145-57; PMID:18497976; http://dx.doi.org/10.3892/ijo_32_6_1145
11. Teixeira J, Maheswaran S, Donahoe PK. Müllerian inhibiting substance: an instructive developmental hormone with diagnostic and possible therapeutic applications. Endocr Rev 2001; 22:657-74; PMID:11588147
12. Durlinger AL, Visser JA, Themmen AP. Regulation of ovarian function: the role of anti-Müllerian hormone. Reproduction 2002; 124:601-9; PMID:12416998; http://dx.doi.org/10.1530/rep.0.1240601
13. Ingraham HA, Hirokawa Y, Roberts LM, Mellon SH, McGee E, Nachtigal MW, Visser JA. Autocrine and paracrine Müllerian inhibiting substance hormone signaling in reproduction. Recent Prog Horm Res 2000; 55:53-67, discussion 67-8; PMID:11036933
14. Sriraman V, Niu E, Matias JR, Donahoe PK, MacLaughlin DT, Hardy MP, Lee MM. Müllerian inhibiting substance inhibits testosterone synthesis in adult rats. J Androl 2001; 22:750-8; PMID:11545286
15. Gupta V, Carey JL, Kawakubo H, Muzikansky A, Green JE, Donahoe PK, MacLaughlin DT, Maheswaran S. Mullerian inhibiting substance suppresses tumor growth in the C3(1)T antigen transgenic mouse mammary carcinoma model. Proc Natl Acad Sci U S A 2005; 102:3219-24; PMID:15728372; http://dx.doi.org/10.1073/pnas.0409709102
16. Segev DL, Ha TU, Tran TT, Kenneally M, Harkin P, Jung M, MacLaughlin DT, Donahoe PK, Maheswaran S. Mullerian inhibiting substance inhibits breast cancer cell growth through an NFkappa B-mediated pathway. J Biol Chem 2000; 275:28371-9; PMID:10874041; http://dx.doi.org/10.1074/jbc.M004554200
17. Hoshiya Y, Gupta V, Segev DL, Hoshiya M, Carey JL, Sasur LM, Tran TT, Ha TU, Maheswaran S. Mullerian Inhibiting Substance induces NFkB signaling in breast and prostate cancer cells. Mol Cell Endocrinol 2003; 211:43-9; PMID:14656475; http://dx.doi.org/10.1016/j.mce.2003.09.010
18. Barbie TU, Barbie DA, MacLaughlin DT, Maheswaran S, Donahoe PK. Mullerian Inhibiting Substance inhibits cervical cancer cell growth via a pathway involving p130 and p107. Proc Natl Acad Sci U S A 2003; 100:15601-6; PMID:14671316; http://dx.doi.org/10.1073/pnas.2636900100
19. Hwang SJ, Suh MJ, Yoon JH, Kim MR, Ryu KS, Nam SW, Donahoe PK, Maclaughlin DT, Kim JH. Identification of characteristic molecular signature of Müllerian inhibiting substance in human HPV-related cervical cancer cells. Int J Oncol 2011; 39:811-20; PMID:21573503
20. Renaud EJ, MacLaughlin DT, Oliva E, Rueda BR, Donahoe PK. Endometrial cancer is a receptor-mediated target for Mullerian Inhibiting Substance. Proc Natl Acad Sci U S A 2005; 102:111-6; PMID:15618407; http://dx.doi.org/10.1073/pnas.0407772101
21. Pieretti-Vanmarcke R, Donahoe PK, Pearsall LA, Dinulescu DM, Connolly DC, Halpern EF, Seiden MV, MacLaughlin DT. Mullerian Inhibiting Substance enhances subclinical doses of chemotherapeutic agents to inhibit human and mouse ovarian cancer. Proc Natl Acad Sci U S A 2006; 103:17426-31; PMID:17088539; http://dx.doi.org/10.1073/pnas.0607959103
22. Pieretti-Vanmarcke R, Donahoe PK, Szotek P, Manganaro T, Lorenzen MK, Lorenzen J, Connolly DC, Halpern EF, MacLaughlin DT. Recombinant human Mullerian inhibiting substance inhibits long-term growth of MIS type II receptor-directed transgenic mouse ovarian cancers in vivo. Clin Cancer Res 2006; 12:1593-8; PMID:16533786; http://dx.doi.org/10.1158/1078-0432.CCR-05-2108
23. Stephen AE, Pearsall LA, Christian BP, Donahoe PK, Vacanti JP, MacLaughlin DT. Highly purified müllerian inhibiting substance inhibits human ovarian cancer in vivo. Clin Cancer Res 2002; 8:2640-6; PMID:12171896
24. Jamin SP, Arango NA, Mishina Y, Hanks MC, Behringer RR. Genetic studies of the AMH/MIS signaling pathway for Müllerian duct regression. Mol Cell Endocrinol 2003; 211:15-9; PMID:14656471; http://dx.doi.org/10.1016/j.mce.2003.09.006
25. Anttonen M, Färkkilä A, Tauriala H, Kauppinen M, Maclaughlin DT, Unkila-Kallio L, Bützow R, Heikinheimo M. Anti-Müllerian hormone inhibits growth of AMH type II receptor-positive human ovarian granulosa cell tumor cells by activating apoptosis. Lab Invest 2011; 91:1605-14; PMID:21808236; http://dx.doi.org/10.1038/labinvest.2011.116
26. Masiakos PT, MacLaughlin DT, Maheswaran S, Teixeira J, Fuller AF Jr., Shah PC, Kehas DJ, Kenneally MK, Dombkowski DM, Ha TU, et al. Human ovarian cancer, cell lines, and primary ascites cells express the human Mullerian inhibiting substance (MIS) type II receptor, bind, and are responsive to MIS. Clin Cancer Res 1999; 5:3488-99; PMID:10589763
27. Segev DL, Hoshiya Y, Hoshiya M, Tran TT, Carey JL, Stephen AE, MacLaughlin DT, Donahoe PK, Maheswaran S. Mullerian-inhibiting substance regulates NF-kappa B signaling in the prostate in vitro and in vivo. Proc Natl Acad Sci U S A 2002; 99:239-44; PMID:11773638; http://dx.doi.org/10.1073/pnas.221599298
28. Bakkum-Gamez JN, Aletti G, Lewis KA, Keeney GL, Thomas BM, Navarro-Teulon I, Cliby WA. Müllerian inhibiting substance type II receptor (MISIIR): a novel, tissue-specific target expressed by gynecologic cancers. Gynecol Oncol 2008; 108:141-8; PMID:17988723; http://dx.doi.org/10.1016/j.ygyno.2007.09.010
29. Rodina AV, Gukasova NV, Makarov VA, Kondrasheva IG, Khomyakova AV, Posypanova GA, Popova ON, Moskaleva EY, Severin SE. Localization of Mullerian inhibiting substance receptors in various human cancer cell lines. Biochemistry (Mosc) 2008; 73:797-805; PMID:18707588; http://dx.doi.org/10.1134/S0006297908070080
30. Song JY, Chen KY, Kim SY, Kim MR, Ryu KS, Cha JH, Kang CS, MacLaughlin DT, Kim JH. The expression of Müllerian inhibiting substance/anti-Müllerian hormone type II receptor protein and mRNA in benign, borderline and malignant ovarian neoplasia. Int J Oncol 2009; 34:1583-91; PMID:19424576
31. Salhi I, Cambon-Roques S, Lamarre I, Laune D, Molina F, Pugnière M, Pourquier D, Gutowski M, Picard JY, Xavier F, et al. The anti-Müllerian hormone type II receptor: insights into the binding domains recognized by a monoclonal antibody and the natural ligand. Biochem J 2004; 379:785-93; PMID:14750901; http://dx.doi.org/10.1042/BJ20031961
32. Krysko DV, Vanden Berghe T, D'Herde K, Vandenabeele P. Apoptosis and necrosis: detection, discrimination and phagocytosis. Methods 2008; 44:205-21; PMID:18314051; http://dx.doi.org/10.1016/j.ymeth.2007.12.001
33. Clémenceau B, Congy-Jolivet N, Gallot G, Vivien R, Gaschet J, Thibault G, Vié H. Antibody-dependent cellular cytotoxicity (ADCC) is mediated by genetically modified antigen-specific human T lymphocytes. Blood 2006; 107:4669-77; PMID:16514054; http://dx.doi.org/10.1182/blood-2005-09-3775
34. Clémenceau B, Vivien R, Pellat C, Foss M, Thibault G, Vié H. The human natural killer cytotoxic cell line NK-92, once armed with a murine CD16 receptor, represents a convenient cellular tool for the screening of mouse mAbs according to their ADCC potential. MAbs 2013; 5:587-94; PMID:23770975; http://dx.doi.org/10.4161/mabs.25077
35. Leone Roberti Maggiore U, Bellati F, Ruscito I, Gasparri ML, Alessandri F, Venturini PL, Ferrero S. Monoclonal antibodies therapies for ovarian cancer. Expert Opin Biol Ther 2013; 13:739-64; PMID:23373587; http://dx.doi.org/10.1517/14712598.2013.767328
36. Chen YG. Endocytic regulation of TGF-beta signaling. Cell Res 2009; 19:58-70; PMID:19050695; http://dx.doi.org/10.1038/cr.2008.315
37. Le Roy C, Wrana JL. Clathrin- and non-clathrin-mediated endocytic regulation of cell signalling. Nat Rev Mol Cell Biol 2005; 6:112-26; PMID:15687999; http://dx.doi.org/10.1038/nrm1571
38. Di Guglielmo GM, Le Roy C, Goodfellow AF, Wrana JL. Distinct endocytic pathways regulate TGF-beta receptor signalling and turnover. Nat Cell Biol 2003; 5:410-21; PMID:12717440; http://dx.doi.org/10.1038/ncb975
39. Ha TU, Segev DL, Barbie D, Masiakos PT, Tran TT, Dombkowski D, Glander M, Clarke TR, Lorenzo HK, Donahoe PK, et al. Mullerian inhibiting substance inhibits ovarian cell growth through an Rb-independent mechanism. J Biol Chem 2000; 275:37101-9;

PMID:10958795; http://dx.doi.org/10.1074/jbc.M005701200
40. Clynes RA, Towers TL, Presta LG, Ravetch JV. Inhibitory Fc receptors modulate in vivo cytotoxicity against tumor targets. Nat Med 2000; 6:443-6; PMID:10742152; http://dx.doi.org/10.1038/74704
41. Hasui M, Saikawa Y, Miura M, Takano N, Ueno Y, Yachie A, Miyawaki T, Taniguchi N. Effector and precursor phenotypes of lymphokine-activated killer cells in mice with severe combined immunodeficiency (scid) and athymic (nude) mice. Cell Immunol 1989; 120:230-9; PMID:2784720; http://dx.doi.org/10.1016/0008-8749(89)90190-1
42. van den Berg-Bakker CA, Hagemeijer A, Franken-Postma EM, Smit VT, Kuppen PJ, van Ravenswaay Claasen HH, Cornelisse CJ, Schrier PI. Establishment and characterization of 7 ovarian carcinoma cell lines and one granulosa tumor cell line: growth features and cytogenetics. Int J Cancer 1993; 53:613-20; PMID:8436435; http://dx.doi.org/10.1002/ijc.2910530415
43. Zhang H, Vollmer M, De Geyter M, Litzistorf Y, Ladewig A, Dürrenberger M, Guggenheim R, Miny P, Holzgreve W, De Geyter C. Characterization of an immortalized human granulosa cell line (COV434). Mol Hum Reprod 2000; 6:146-53; PMID:10655456; http://dx.doi.org/10.1093/molehr/6.2.146
44. Wahyono D, Piechaczyk M, Scherrmann JM, Girard C, Grenier J, Mani JC, Bastide JM, Pau B. Highly specific radioimmunoassay for digoxin using a monoclonal antibody selected for lack of interference by digoxin-like immunoreactive substances in cord blood sera. Ther Drug Monit 1991; 13:113-9; PMID:2053117; http://dx.doi.org/10.1097/00007691-199103000-00005
45. Hammarstrom S, Shively JE, Paxton RJ, Beatty BG, Larsson A, Ghosh R, Bormer O, Buchegger F, Mach JP, Burtin P, et al. Antigenic sites in carcinoembryonic antigen. Cancer Res 1989; 49:4852-8; PMID:2474375
46. Tavassoli FAaD. P., ed. Pathology and Genetics of tumors of the breast and female genital organs, 2003.